

Protein Science

Electrostatic contributions drive the interaction between *Staphylococcus aureus* protein Efb-C and its complement target C3d

Nurit Haspel, Daniel Ricklin, Brian V. Geisbrecht, Lydia E. Kaviraki and John D. Lambris

Protein Sci. 2008 17: 1894-1906; originally published online Aug 7, 2008;
Access the most recent version at doi:[10.1110/ps.036624.108](https://doi.org/10.1110/ps.036624.108)

Supplementary data

"Supplemental Research Data"
<http://www.proteinscience.org/cgi/content/full/ps.036624.108/DC1>

References

This article cites 52 articles, 15 of which can be accessed free at:
<http://www.proteinscience.org/cgi/content/full/17/11/1894#References>

Email alerting service

Receive free email alerts when new articles cite this article - sign up in the box at the top right corner of the article or [click here](#)

Notes

To subscribe to *Protein Science* go to:
<http://www.proteinscience.org/subscriptions/>

Electrostatic contributions drive the interaction between *Staphylococcus aureus* protein Efb-C and its complement target C3d

NURIT HASPEL,^{1,4} DANIEL RICKLIN,^{2,4} BRIAN V. GEISBRECHT,^{3,5} LYDIA E. KAVRAKI,^{1,5}
AND JOHN D. LAMBRIS^{2,5}

¹Department of Computer Science, Rice University, Houston, Texas 77005, USA

²Department of Pathology and Laboratory Medicine, University of Pennsylvania, Philadelphia, Pennsylvania 19104, USA

³Division of Cell Biology and Biophysics, School of Biological Sciences, University of Missouri at Kansas City, Kansas City, Missouri 64110, USA

(RECEIVED May 29, 2008; FINAL REVISION May 29, 2008; ACCEPTED July 28, 2008)

Abstract

The C3-inhibitory domain of *Staphylococcus aureus* extracellular fibrinogen-binding protein (Efb-C) defines a novel three-helix bundle motif that regulates complement activation. Previous crystallographic studies of Efb-C bound to its cognate subdomain of human C3 (C3d) identified Arg-131 and Asn-138 of Efb-C as key residues for its activity. In order to characterize more completely the physical and chemical driving forces behind this important interaction, we employed in this study a combination of structural, biophysical, and computational methods to analyze the interaction of C3d with Efb-C and the single-point mutants R131A and N138A. Our results show that while these mutations do not drastically affect the structure of the Efb-C/C3d recognition complex, they have significant adverse effects on both the thermodynamic and kinetic profiles of the resulting complexes. We also characterized other key interactions along the Efb-C/C3d binding interface and found an intricate network of salt bridges and hydrogen bonds that anchor Efb-C to C3d, resulting in its potent complement inhibitory properties.

Keywords: proteins of the immune system; structure; computational analysis of protein structure; molecular mechanics/dynamics; thermodynamics; hydrodynamics; complement; Efb-C; electrostatics

Supplemental material: see www.proteinscience.org

The remarkable ability of the human body to defend itself against microbial intruders is predicated upon a myriad of complex interactions between components of both the innate and adaptive branches of the immune system. In this respect, the complement system constitutes a vital first-response mechanism that both quickly recognizes and eliminates foreign cells while also stimulating the

downstream inflammatory and adaptive immune responses that are essential to combating such infections. The third complement component (C3) has long been recognized as the central element in this cascade, since it serves as a “hub,” where all three activation pathways converge (classical, lectin, and alternative pathway), and through which all downstream effector activities are initiated (Sahu and Lambris 2001). In this process, native C3 (184 kDa) is cleaved into its two active fragments, C3a (9 kDa) and C3b (175 kDa), by multiprotein enzyme complexes (C3 convertases). While the anaphylatoxin C3a induces pro-inflammatory responses and may also disrupt bacterial membranes (Nordahl et al. 2004), C3b is covalently attached to hydroxyl- and amine-rich surfaces

⁴These authors contributed equally to this work.

⁵These authors shared the supervision of this study.

Reprint requests to: John D. Lambris, University of Pennsylvania, 40 Stellar Chance, Philadelphia, Pennsylvania 19104, USA; e-mail: Lambris@upenn.edu; fax: 215-573-8738.

Article and publication are at <http://www.proteinscience.org/cgi/doi/10.1110/ps.036624.108>.

in close proximity of sites of activation. This reactivity is maintained by exposition and activation of a previously buried thioester bond during the cleavage of C3 (Sahu and Lambris 2001; Janssen et al. 2006). Opsonization by C3b amplifies complement activation and leads to a number of antimicrobial activities such as phagocytosis and formation of the pore-like membrane attack complex (MAC). In order to control complement activation and prevent opsonization of host cells, a set of regulators interfere with the formation of convertase and MAC and degrade C3b in a two-step process to C3c (135 kDa) and C3d (40 kDa). While the inactive C3c fragment is released from the surface, the thioester-containing C3d remains firmly attached and acts as a bridge to the adaptive response via stimulation of B cells (Carroll 2000).

Throughout the millennia of co-evolution between microorganisms and their human hosts, many pathogens from diverse kingdoms of life have acquired an impressive and elaborate arsenal of immunomodulatory proteins. In this respect, the bacterium *Staphylococcus aureus* expresses a particularly large cohort of evasion proteins that inhibit several key aspects of the immune response including complement (Foster 2005; Chavakis et al. 2007; Lambris et al. 2008). The extracellular-fibrinogen binding protein (Efb) is one of several complement inhibitors expressed by *S. aureus*. Aside from its eponymous interaction with fibrinogen, the protease-resistant, carboxy-terminal domain (Efb-C) of this 16-kDa protein inhibits complement activation by interacting with C3 and its thioester-containing fragments (C3b, iC3b, C3d) (Lee et al. 2004a, b; Hammel et al. 2007b). We recently reported the crystal structures of Efb-C both free and bound to its cognate subdomain from C3 (i.e., C3d) (Fig. 1A; Hammel et al. 2007b). Subsequent structure/function analysis demonstrated that binding of Efb-C to either native C3 or C3b induced conformational changes (Hammel et al. 2007b) that rendered these proteins incapable of participating in downstream activities associated with the C3b-containing convertases of the alternative pathway (Hammel et al. 2007b; Jongerius et al. 2007). Although the precise nature of these Efb-C-induced conformational changes is not currently understood, their importance was underscored by the identification of a distinct *S. aureus* protein, Ehp, which appears to induce similar changes that likewise, culminate in potent inhibition of alternative pathway associated convertases (Hammel et al. 2007a; Jongerius et al. 2007). Thus, it appears that this alternative pathway-specific inhibitory mechanism, defined originally by Efb-C, makes an important overall contribution to evasion of complement by *S. aureus*.

Given the involvement of complement in many autoimmune, inflammatory, or ischemic diseases, inhibition of the cascade at the level of C3 has long been considered a promising therapeutic approach (Ricklin and Lambris

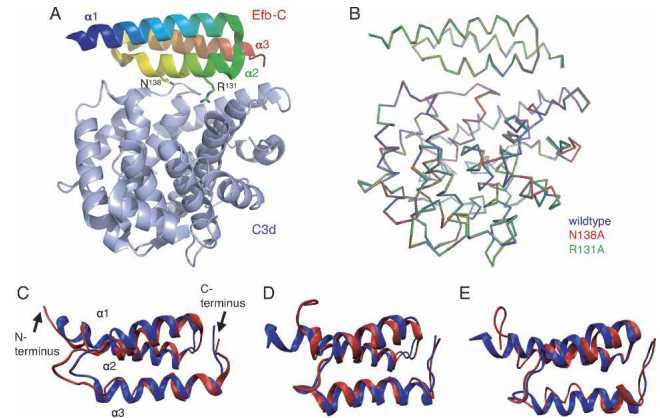


Figure 1. Impact of alanine mutations at Efb-C residues Arg-131 and Asn-138 on the crystal structure of the Efb-C/C3d complex. (A) Cartoon representation of the cocystal (PDB accession code 2GOX) between human C3d (pale blue) and wild-type Efb-C (spectrum). The three helices of Efb-C ($\alpha 1$, $\alpha 2$, $\alpha 3$) and the sites of mutation (R131 and N138; stick representation) are highlighted in the structure. (B) Aligned backbone traces of the crystallized C3d complexes with Efb-C wild type (blue) as well as mutants R131A (green) and N138A (red). No significant changes in the overall structure could be detected between the three complexes, suggesting that the mutations do not induce any significant conformational changes at the Efb-C/C3d interface. Snapshots of the Efb-C conformations in the equilibrated state (blue) and after 20 nsec of the simulation (red): (C) wild type, (D) R131A, and (E) N138A. Although the entire complex was simulated, only Efb-C is shown here for clarity, as C3d exhibited relatively little change during the simulation.

2007a). Owing to its high inhibitory potency, Efb-C represents an attractive platform for the development of complement-specific therapeutics. To approach this elusive goal, a comprehensive understanding of the Efb-C/C3d interface in terms of both its structure and the precise contributions of individual residues is of central importance. Previous structural analyses of the binding site using both crystallographic and solution mass spectrometry methods have identified a surprisingly small number of residues in Efb-C that form the cornerstone of this kinetically and energetically stable complex (Hammel et al. 2007b; Chen et al. 2008). Specifically, Arg-131 and Asn-138 (highlighted in Fig. 1A) were found to form a large number of discrete contacts with C3d, and simultaneous mutation of both residues to either alanine (RA/NA) or glutamic acid (RE/NE) resulted in a complete loss of both C3d binding and complement inhibition (Hammel et al. 2007b). In addition, the atypically large overall positive charge of Efb-C ($pI \approx 10$) and the location of its binding site at the periphery of an evolutionarily conserved and predominantly acidic pocket on C3d (Nagar et al. 1998) suggested that there may be a substantial electrostatic contribution to either forming and/or maintaining this inhibitory complex. Although such electrostatic interactions are not uncommon in protein-protein interactions, they are paramount in a number of key

interactions involving C3 and other proteins of the complement system (Morikis and Lambris 2004; Sfyroera et al. 2005). Finally, mutation of the two key residues also could have altered the local structure of the Efb-C protein, and their simultaneous replacement might have led to synergistic or deleterious effects.

To further define the driving forces behind this important protein–protein interaction, we employed a multidisciplinary combination of structural, biophysical, and computational methods to analyze the energetics and kinetics of the C3d interaction with wild-type Efb-C and its single mutants R131A and N138A. While the conformational arrangement of individual complexes was assessed by X-ray crystallography, we used isothermal titration calorimetry (ITC) and surface plasmon resonance (SPR) to study the influence of individual mutations on the thermodynamic interaction profile and the complex formation/stability, respectively. Furthermore, an ensemble of computational approaches allowed us to characterize the short-range time-related behavior of the Efb-C/C3d complexes, estimate their free energy of binding, and identify additional pairwise interactions in the binding interface. Our results not only confirm the importance of each of the individual key residues but also demonstrate that electrostatic contributions are highly important for the interaction of the bacterial inhibitor with its target in the complement system. In this respect, our study represents a valuable contribution to both the characterization of molecular complement evasion mechanisms and the development of Efb-based therapeutics.

Results

Loss of the Efb-C side chains at positions Arg-131 and Asn-138 does not significantly influence the structure of their complexes with C3d

To address the molecular basis of the Efb-C/C3d interaction more thoroughly, we expressed and purified the Efb-C single mutants R131A and N138A. Although prior studies revealed that loss of both residues simultaneously resulted in a nonfunctional Efb-C protein (Hammel et al. 2007b), both of these mutants form stable 1:1 complexes with C3d that could be efficiently reconstituted and isolated by gel-filtration chromatography (data not shown). Further, each of these complexes produce crystals in the space group $P4_1$ that diffracted to 2.3 Å (R131A) and 2.1 Å (N138A) limiting resolution, both of which are comparable to those produced by wild-type Efb-C (Table 1; Fig. 1A). The resulting structures were solved by molecular replacement and the refined models were superimposed upon the wild-type Efb-C complex (Table 1; Fig. 1B; Hammel et al. 2007b). Analysis of structural deviations by inspection revealed that neither

Table 1. Data collection statistics, structure determination, and refinement

	R131A/C3d	N138A/C3d
	Data collection	
Space group	$P4_1$	$P4_1$
Unit cell dimensions (Å)	$a = b = 90.89,$ $c = 122.83$	$a = b = 91.01,$ $c = 120.52$
Complete complexes/ASU	2	2
Resolution limits (Å)	50–2.3	50–2.1
Completeness (%)	99.7 (98.9)	99.6 (96.8)
Unique reflections	45,612	56,794
Redundancy	3.8	3.6
R_{merge} (%) ^a	10.0 (41.3)	10.3 (41.5)
$\langle\langle I \rangle\rangle / \langle\langle \sigma I \rangle\rangle$	12.2 (3.0)	10.4 (2.5)
	Refinement statistics	
$R_{\text{cryst}}/R_{\text{free}}$ (%) ^b	20.4/21.8	21.8/24.1
RMSD from ideality		
Bond length (Å)	0.007	0.006
Bond angle (°)	1.304	1.174
Ramachandran core (disallowed) (%)	92.2 (0)	92.8 (0)
Average B factor, all atoms (Å ²)	42.4	41.1
Average B factor, solvent (Å ²)	37.3	38.4
Protein atoms modeled	5712	5718
Ordered solvent molecules	140	150

^a $R_{\text{merge}} = \sum_i \sum_h |I_i(h) - \langle I(h) \rangle| / \sum_i \sum_h I_i(h)$, where $I_i(h)$ is the i th measurement of reflection h and $\langle I(h) \rangle$ is a weighted mean of all measurements of h .

^b $R = \sum_h |F_{\text{obs}}(h) - F_{\text{calc}}(h)| / \sum_h |F_{\text{obs}}(h)|$. R_{cryst} and R_{free} were calculated from the working and test reflection sets, respectively. The test set constituted 5% of the total reflections not used in refinement.

the Efb-C nor C3d polypeptides in either complex showed any significant change in their overall structures. Consequently, the calculated root mean square deviation (RMSD) values for the C α positions between the mutant and wild-type complexes were very low (0.12 Å and 0.24 Å for R131A and N138A, respectively). Together, these findings demonstrate that loss of the side chain alone at either of these C3d contact sites is insufficient to perturb the overall structure of the resulting complexes.

Although crystallographic analysis is an invaluable tool in understanding macromolecular interactions, important but subtle changes in protein conformation and dynamics may be undetectable in many cases due to the static nature of the technique. Thus, to approach these issues from an independent perspective, we used a 20-nsec molecular dynamics (MD) simulation to analyze changes in the structures of the mutant Efb-C complexes. Figure 1C–E shows the Efb-C wild type and two mutants in the equilibrated state and at the end of the simulation. Notice that while the entire Efb-C/C3d complex was simulated, C3d is omitted from the figure for clarity. Both the wild type and the mutants became structurally rearranged to an extent. In all three cases, the N-terminal loop and the $\alpha 2$ – $\alpha 3$ loop, which is close to the binding site and connects helices $\alpha 2$ and $\alpha 3$, represented the most flexible areas.

Nevertheless, simulation trajectories revealed that both the wild-type Efb-C and the mutants in question could form structurally stable complexes, which is consistent with the experimental data presented above. As might be expected from loss of these contributing side chains, the potential energy estimate for the native complex is significantly lower than that of N138A/C3d, which in turn is lower than R131A/C3d (Fig. 2A). Investigation of the RMSD evolution during the MD simulation time course can also be an informative approach for comparison of the wild-type and mutant Efb-C/C3d complexes. In the case of the C3d component, the protein maintained essentially the same structure throughout the simulation as judged by an RMSD of ~ 2 – 3.5 Å in all three complexes (Fig. 2B). The Efb-C proteins were also rather stable structurally and remained mostly within 1.5–2 Å throughout the course of the simulation (Fig. 2C).

The R131A and N138A mutations affect both the thermodynamic and kinetic profiles of Efb-C interaction with C3d

Though the final differences in the $\alpha 2$ – $\alpha 3$ loop conformation observed in the Efb-C mutants appeared minor, they nevertheless suggested that the loss of these side chains might affect additional biochemical properties that govern either the association or dissociation of the

complex. As a result, we examined the impact of both the R131A and N138A mutations on the thermodynamic and kinetic profiles of the Efb-C/C3d interaction through ITC and SPR, respectively. Both mutants show significant calorimetric binding that could be fit to a single set of sites with 1:1 stoichiometry, though each is significantly weaker than that reported for wild-type Efb-C, but not as diminished as the previously studied R131A/N138A double mutant (Fig. 3A; Hammel et al. 2007b). This loss in affinity is slightly larger for R131A (13-fold) than for N138A (10-fold), with the enthalpy following the same trend (2.2- and 1.5-fold, respectively). Extraction of the relevant thermodynamic constants (ΔG , $T\Delta S$; Table 2) for each titration revealed that both enthalpic and entropic terms are responsible for the observed affinity differences. The clear effect on the enthalpy values is consistent with a reduction in the number or quality of individual contacts at the binding site, whereas the increase in binding entropy, on the other hand, may be due to entropy/enthalpy compensations in the weakened complex.

We further estimated the average free energy of binding for the three complexes obtained by the MD simulations using the mm-pbsa/gbsa approach implemented in the AMBER package (Kollman et al. 2000). Table 3 shows the computational estimate of free energy for all the simulated complexes and the decomposition of the free energy according to individual components. While all three complexes show favorable binding, the free energy estimate for the native complex is significantly lower than the N138A mutant, which in turn is lower than the R131A mutant. Even though the absolute values for ΔH deviate significantly from the ITC-derived constants, the relative differences closely reflect the trend observed in the biophysical analysis (Tables 2 and 3). The discrepancy in the absolute numbers for ΔH and ΔG can largely be attributed to the approximations used in the simulation, such as implicit solvent and interaction distance cutoff (see Materials and Methods). It should be noted that the General Born (GB) approximation is known to underestimate the free energy due to inaccuracies in estimating the first solvation shell effects (Bonnet and Bryce 2005). GB deviates from the slower but more accurate Poisson-Boltzmann approach, especially when calculating the free energies of species with net charge (Edinger et al. 1997), such as these complexes. The differences between the experimental observations and the calculations could be decreased by changing the igb parameter of the mm-pbsa/gbsa program to 5 (Onufriev et al. 2004). However, we found that in that case the error was in the order of magnitude of the calculated energy. Entropy calculations are not included in this section: They are extremely demanding computationally, especially for a system this size, and the protocol we used provides only a very rough approximation (see Materials

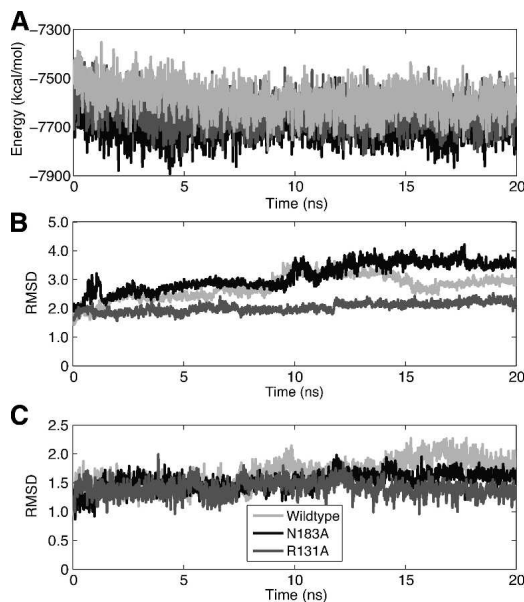


Figure 2. Evolution of the RMSD and potential energy of the different components of the wild type and the two mutant complexes during the simulation. (A) Potential energy plot of the three complexes during the simulation. The RMSD of C3d (B) and Efb-C (C) were measured with respect to the minimized C3d and Efb-C of each one of the complexes, respectively. Hydrogen atoms were not included in the measurement. There is a difference in scale on the y-axis between A, B, and C.

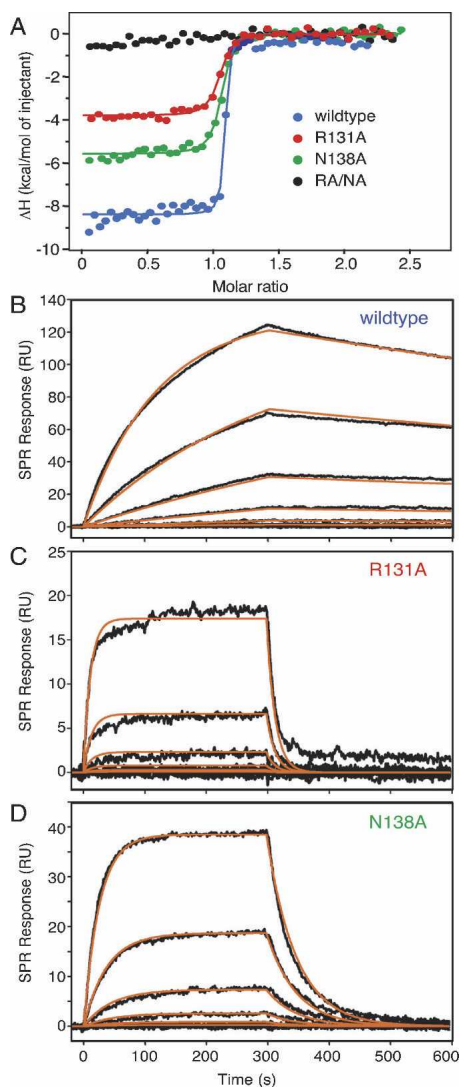


Figure 3. Characterization of the binding properties between C3d and three Efb-C proteins (wild type, R131A, and N138A) by ITC (A) and SPR (B–D). (A) Calorimetric determination of the binding enthalpy and affinity by injecting Efb-C proteins (150 μ M) into C3d (12 μ M). (B–D) Kinetic profiling of Efb-C wild type (B), R131A (C), and N138A (D) by injecting a twofold C3d dilution series (0.27–22 nM) over immobilized Efb-C proteins (215–240 RU). Black lines represent processed SPR binding signals that have been fitted to Langmuir 1:1 kinetic models (red lines). Binding constants from both the ITC and SPR experiments are summarized in Table 2.

and Methods). Decomposition of the free energy into individual components allowed further conclusions about the nature of the Efb-C/C3d interaction. In agreement with our previous observations (Hammel et al. 2007b) and the resulting binding hypothesis, the electrostatic component (E_{elec}) dominates the binding in all cases (Table 2). While van der Waals contributions (E_{vdw}) still play a significant role, their absolute values are significantly lower. As expected, the electrostatic energy is more

affected by the R131A than by the N138A mutation (34% and 15% decrease, respectively).

The loss of the Arg-131 and Asn-138 side chains results in pronounced effects on the thermodynamic stability of the Efb-C/C3d complex. In principle, these effects may be due to disruption of either association or dissociation of the complex; therefore it seemed reasonable that they may also be manifested as changes in the kinetic rate constants associated with this interaction. To test this hypothesis, we compared the kinetic profiles of the mutant and wild-type complexes by SPR. Analysis of the C3d interaction with immobilized Efb-C proteins reveals the same affinity ranking as ITC (Table 2). Furthermore, the calculated K_d values correspond closely between the two methods (which served as an internal validation of the results). All three interaction sets were clearly concentration dependent and show a close fit to a Langmuir 1:1 kinetic model (Fig. 3B–D). A direct comparison of the kinetic rate constants (Table 2) reveals that the dissociation rate constants (k_{off}), which are closely linked to the stability of the established complex, are affected to a far greater extent by the binding-site mutations than are the association rate constants (k_{on}). Similarly to the other thermodynamic parameters, the effects on the kinetic rate constants follow a common trend, but are more pronounced for the R131A when compared to the N138A mutant. In sum, these kinetic data strongly suggest that complex destabilization by a reduced contact network is the driving force behind the loss in affinity, as opposed to a disruption in complex formation.

Binding properties of Efb-C are influenced by electrostatic changes

Based on the energy calculations in this study and on previous reports (Hammel et al. 2007b; Chen et al. 2008), we hypothesized that the binding of Efb-C to C3d is predominantly electrostatic in nature. As shown by the electrostatic potential surfaces of C3d, Efb-C and its N138A and R131A mutants at the equilibrated state (Fig. 4A–C), Efb-C and the two mutants are characterized by a large cloud of positive charge around most of $\alpha 1$ and $\alpha 2$ helices and the $\alpha 2$ – $\alpha 3$ loop in the direction of the binding region with C3d. A smaller cloud of negative charge encompasses helix $\alpha 3$. C3d is an overall neutral molecule, but the charge is well separated so that the area around its binding site is negative (as seen in Fig. 4D). This creates strong electrostatic attraction that enables initial binding.

In order to further test the influence of electrostatic contributions to the formation and stability of the Efb-C/C3d complex, we repeated the kinetic experiments in running buffers of increasing NaCl concentration (10 mM sodium phosphate, 75–600 mM sodium chloride). As shown in Figure 5, each doubling of the salt concentration had a direct effect on the signal intensity and binding

Table 2. Binding constants of C3d interactions with Efb-C and its R131A and N138A mutants by isothermal titration calorimetry (ITC) and surface plasmon resonance (SPR)

Efb-C species	K_d ITC (nM)	ΔH (kcal/mol)	$T\Delta S^a$ (kcal/mol)	ΔG^a (kcal/mol)	k_{on} ($10^5 M^{-1}sec^{-1}$)	k_{off} ($10^{-4} sec^{-1}$)	K_d SPR (nM)
Wild type	2 ± 1	-8.5	3.4	-11.9	4.04 ± 0.96	5.63 ± 0.94	1.4 ± 0.1
R131A	26 ± 6	-3.9	6.4	-10.3	13.3 ± 8.5	687 ± 188	62.1 ± 32.4
N138A	19 ± 4	-5.5	5.0	-10.5	12.0 ± 6.6	214 ± 45	19.8 ± 6.0

^aCalculated from the equation $\Delta G = \Delta H - T\Delta S = RT \ln K_d$ with $T = 298.15$ K (25°C).

kinetics (a more detailed analysis of the kinetic changes is available in Supplemental Figures 1 and 2). In case of the wild type, the increase in ionicity mostly affected the association phases, with the highest complex formation at lowest NaCl concentration. The dissociation phase, on the other hand, was generally less influenced in the wild type, and a salt increase from 75 to 300 mM even seemed to slightly enhance complex stability. Interestingly, both mutants showed a different sensitivity toward ionic strength than the wild-type Efb-C. Here, increasing salt concentration seemed to weaken the complex (manifesting in a faster dissociation rate) while the effects on the complex association are less clear. However, the lower binding intensities and the resulting unfavorable signal-to-noise ratio make an accurate assessment of these trends more difficult than for the wild type.

When considering the large effects on the association rates, electrostatic complementarity and attraction seem to be of high importance for the initial complex formation in the wild type. While Arg-131 (and Asn-138) may contribute to this effect to some extent, they do not seem to be essential in these assembly steps. This suggests that the overall electrostatic potential, which is still highly positive in both mutants, rather than individual ion pairs at the binding interface, is important in this context. Arg-131 and Asn-138 are not essential to the initial binding, but once the complex is formed, both residues are crucial for maintaining its stability. This observation is in good agreement with the theory of “electrostatic steering,” in which long-range electrostatic effects are mainly responsible for enhancing complex formation based on electrostatic complementarity of the binding partners, while short-range electrostatics formed by individual ion pairs

and H-bonds mainly influence the stability of the complex (Sinha and Smith-Gill 2002).

A network of interactions along the binding interface contributes to the strong complex binding

The observation that Arg-131 and Asn-138 serve to stabilize Efb-C/C3d from dissociation, but are not sufficient to the formation of this interaction suggested that additional residues donated by Efb-C may serve important, yet unappreciated roles in maintenance of this complex. To further describe the binding interface and to identify additional key residues, we estimated the contributions of individual amino acids and pairwise interactions to the free energy of binding using MD and the mm-pbsa/gbsa approach described above (Kollman et al. 2000). These methods enabled the decomposition of the overall binding free energy into individual contributions per residue or interaction pair, which in turn permitted the estimation of the associated free energy. This estimate can help prioritize which residues and interactions contribute most to the binding of Efb-C to C3d and can be used as a basis to identify molecular motifs that capture the essential components necessary for recapitulating Efb-C/C3d binding. Figure 6 shows the individual contributions to the complex binding for each residue of C3d (Fig. 6A) as well as for wild-type Efb-C (Fig. 6B) and the two mutants (Fig. 6C,D). Detailed energy values of all the residues in Efb-C and on the binding loops of C3d are provided in Supplemental Tables 1 and 2. Notice that these calculations focused on individual contributions and are distinct from the total free energy calculations done previously in this section.

Table 3. Free energy of binding for the three complexes by analyzing the molecular dynamics trajectory using the mm-pbsa/gbsa approach

Efb-C species	E_{vdw}	E_{elec}	$E_{MM,total}^a$	G_{solv}	ΔH^b
Wild type	-130.87 ± 8.92	-1019.34 ± 56.50	-1150.21 ± 56.92	1039.15 ± 49.36	-111.06 ± 15.58
R131A	-119.66 ± 9.04	-755.77 ± 55.79	-875.43 ± 57.40	781.18 ± 52.25	-94.25 ± 14.96
N138A	-126.73 ± 9.20	-885.18 ± 60.45	-1011.91 ± 63.38	905.85 ± 60.03	-106.06 ± 13.11

All measurements are in kcal/mol.

^aCalculated from the equation $E_{MM,total} = E_{VDW} + E_{elec}$.

^bCalculated from the equation $\Delta H = E_{MM,total} + G_{solv}$.

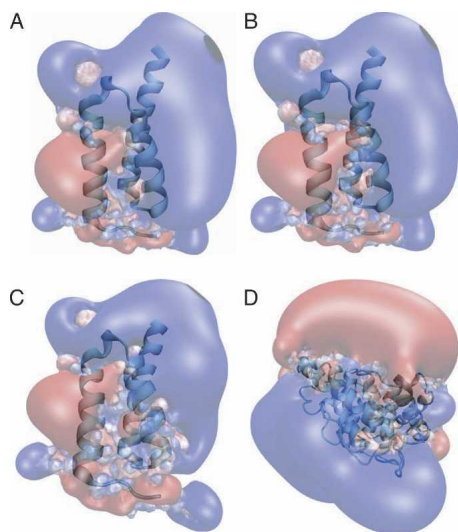


Figure 4. Electrostatic potential surfaces of wild type Efb-C (A), N138A mutant (B), R131A mutant (C), and C3d (D). Iso-surfaces are shown at ± 1 kT/e. Red indicates negative charge and blue indicates positive charge. The molecules are drawn as ribbons.

In order to limit the computational effort, no entropy calculations were included in this approach. Notable contributing residues are labeled in Figure 6. As expected, the most contributing residues on C3d are located on the three binding loops, approximately encompassing residues 1029–1050, 1089–1098, and 1157–1166, respectively. On Efb-C, the majority of the contributing amino acids are located on helix $\alpha 2$, which has the largest interface with C3d. Other significantly contributing residues are Lys-106, Lys-110, and Arg-165, all of which participate in multiple salt bridges with negative residues on the C3d molecule. A number of hydrophobic residues (e.g., Val-127 in Efb-C or Ile-1095 in C3d) also contribute significantly to the binding energy, which can be due to either hydrophobic interactions or to H-bonds involving their backbone. With the exception of the mutated residues themselves, the individual contributing residues in the N138A and R131A mutants show a pattern very similar to wild-type Efb-C. In agreement with the experimental data, the contribution of Arg-131 to the overall binding was found to be exceptionally strong. As seen in Figure 6B,C, disruption of this amino acid impairs complex stability, as demonstrated in the less favorable binding energy of the R131A complex. Apparently, Asn-138 contributes less to the binding than Arg-131.

Significant pairwise contributions to the interaction free energy and a full map of all the interactions involving the three binding loops of C3d are represented in Table 4 and Figure 7, respectively. Each dot in the figure represents a notable interaction, where only interactions with calculated energies lower than -1.5 kcal/mol are

shown. The colors of the dots represent the strength of the interaction and lie on the red–blue range, where shades of red indicate a weaker interaction and shades of blue indicate a stronger interaction. Here, as with the individual contributions, entropy was not calculated. Notably, previously identified contact residues on Efb-C (Lys-106, Lys-110, Arg-131, Lys-135, Asn-138, Lys-148) (Hammel et al. 2007b) were also found to provide notable contributions in the *in silico* study, further validating our results. In addition to these known interactions we found other significant interactions, mainly salt bridges and H-bonds, the most important of which are summarized in Table 4. Notice that many of the interactions are bifurcated, i.e., with two or more adjacent amino acids involved. In this case the energy shown in the table is the sum of the two or more interactions. For example, the last entry in the table is the sum of two interactions:

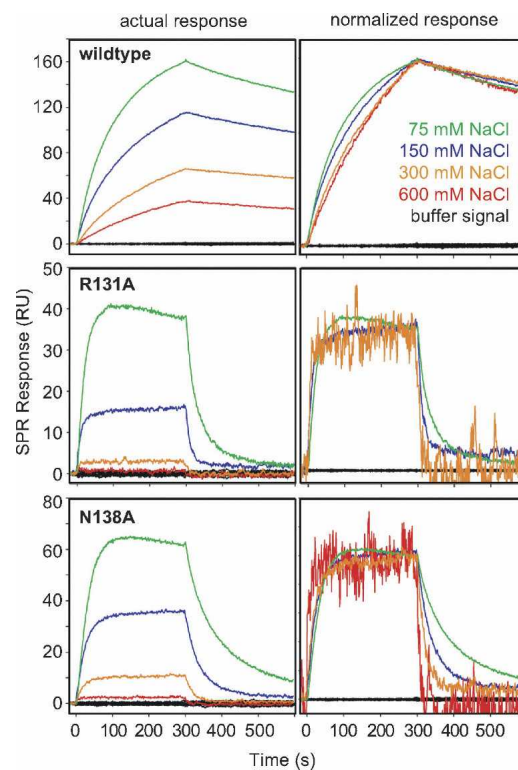


Figure 5. Electrostatic titration experiment using SPR. C3d (22 nM) was injected over immobilized Efb-C proteins (wild type, R131A, and N138A) in 10 mM phosphate buffer (pH 7.4) of increasing sodium chloride concentration (75, 150, 300, 600 mM NaCl). The influence of buffer ionicity is clearly visible in the absolute signal intensity of the SPR response at constant C3d concentration (*left* panels). In order to better visualize the differential effect on association and dissociation phase, the signals have been normalized at injection end (300 sec) by adjusting the maximum intensity to 100 RU (*right* panels). In the case of R131A, the curve at highest salt concentration has not been normalized due to the lack of detectable binding.

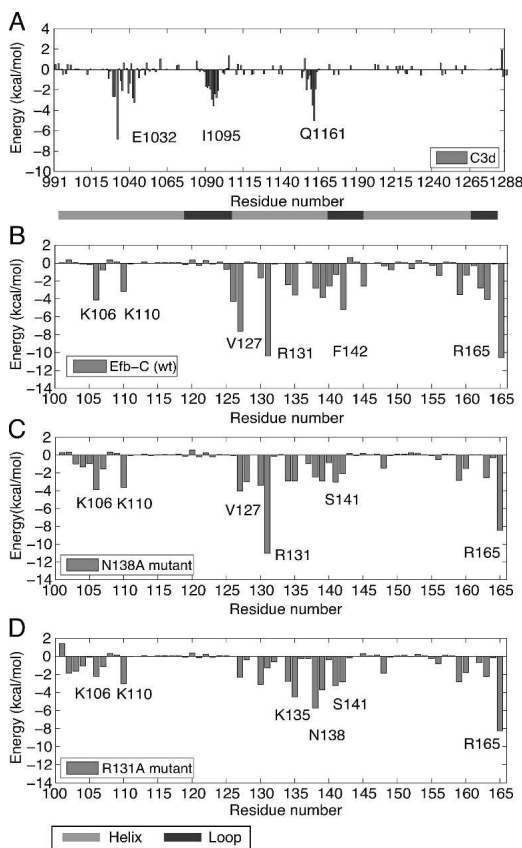


Figure 6. Energetic contribution of individual residues to the binding energy of the C3d/Efb-C complex: (A) C3d, (B) wild-type Efb-C, (C) Efb-C N138A, (D) Efb-C R131A. Notice the difference in scale in the y-axis. Notable contributions are indicated in the figures. Only the C3d molecule of the wild-type Efb-C/C3d complex is shown in panel A. The C3d molecules of the N138A and R131A mutants were omitted, as they show a very similar pattern.

Arg-165/Glu-1032 and Arg-165/Glu-1035, both present at the same time.

The visible pattern emerging from the interaction analysis suggests that nearly every residue on Efb-C that faces the binding site is charged or capable of H-bonding, and involved in some significant interaction. Since Efb-C is a helical protein, nearly one in every three or four residues faces the binding site. It is interesting to note that the interactions with the largest energetic contribution (Lys-106,110/Glu-1159,1160, Arg-131/Asp-1029,Glu-1030, Lys-148/Asp-1096, and Arg-165/Glu-1032,1035; highlighted in boldface in Table 4) are building four networks of salt bridges. These are located on helix α 1, helix α 2, the α 2- α 3 loop, and the C terminus, respectively (see also Fig. 1 for the definition of the helices). The corresponding residues in C3d are located on the three binding loops. Therefore, these networks of salt bridges anchor the Efb-C to the three binding site loops of C3d very strongly (Fig. 7D). The identification of several pairs with similar or even lower

binding energies (Table 4) suggests that disruption of these other interactions may have similar effects.

Discussion

Previous work on the Efb-C/C3d co-crystal structure identified Arg-131 and Asn-138 as two residues within Efb-C that are crucial for the affinity and activity of this bacterial inhibitor (Hammel et al. 2007b). Furthermore, the Efb-C binding site was localized to an area on the C3d surface within close proximity to a highly conserved, acidic pocket (Nagar et al. 1998). The strong positive overall charge of Efb-C led to the hypothesis that this interaction is largely driven by electrostatic contributions. In this study we characterized the contribution of various structural, thermodynamic, and kinetic aspects to the interaction and how they are influenced by mutation of the key residues. Both the computational and biophysical analysis of the individual complexes showed that neither of the mutations studied here significantly affected the overall structure of either Efb-C or its complex with C3d. However, both Efb-C mutants (R131A, N138A) displayed a reduced affinity for their C3d target. This effect is clearly derived from a reduction of individual contacts (e.g., H-bonds and salt bridges), which is manifested on a macromolecular level by a loss of complex stability, as judged by an increase in observed dissociation rates following mutation. Furthermore, in agreement with our considerations of the electrostatic complementarity between the largely cationic Efb-C and the negatively charged acidic pocket

Table 4. Contribution to free energy of binding by the most contributing specific pairwise interactions

Interaction pair residues		Free energy of binding (kcal/mol)		
Efb-C	C3d	Wild type	N138A	R131A
R131	D1029,E1030	-19.53	-17.67	N/A
R131	N1091	-3.41	-4.49	N/A
N138	I1093,A1094,I1095	-5.37	N/A	-6.81
K135	D1156	-5.80	-4.58	-6.51
K145	D1156	-7.33	-4.02	-2.97
K148	I1095,D1096,S1097	-10.08	-13.17	-13.07
D156	K1050	-6.30	-2.48	-4.67
K106	E1159,E1160	-11.51	-9.46	-8.03
K110	E1159,E1160	-9.86	-8.34	-7.41
R165	E1032,E1035	-21.52	-20.36	-12.26
T126,V127	D1029-E1032	-18.87	-8.12	-1.77

In each interaction, the first set of amino acids belongs to Efb-C and the second to C3d. Where the interaction is bifurcated, the sum of the individual interactions is shown. Only interactions that appear in all the three complexes (not including mutated residues) or interactions whose energy is lower than -4 kcal/mol are displayed in the table. Particularly strong interactions (approximately -10 kcal/mol or less) are shown in bold. The complete set of pairwise interactions with binding energies below -1.5 kcal/mol is shown in Figure 7.

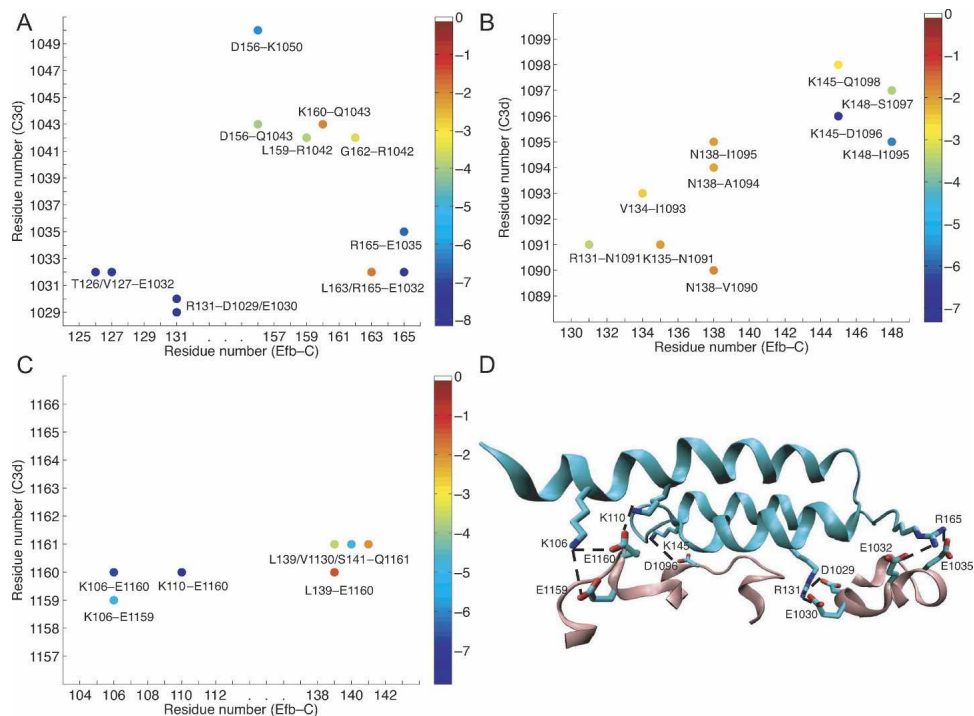


Figure 7. Contribution of pairwise interactions to the binding energy of the native C3d/Efb-C. Each panel depicts the interactions involving one of the three binding loops of C3d, i.e., residues 1029–1050 (A), 1089–1098 (B), and 1157–1166 (C). Favorable interactions are displayed in different shades on the red–blue scale with blue shades indicating lowest energy (see color bar). While interactions with energies higher than -1.5 kcal/mol are not shown, some very low energy values were truncated at -8 kcal/mol up to allow clearer display. (D) Some of the favorable interactions between C3d (pink) and wild-type Efb-C (green). These interactions are marked in boldface in Table 4.

within C3d, the long-range electrostatic contributions were found to play a major role in the initial encounter of the complex. Mutation of Arg-131 and Asn-138 affected the overall electropositive potential of Efb-C only slightly, and the observed effects on complex formation were similarly minor, as judged by the comparable kinetic on-rates for all Efb-C proteins investigated here. Supporting these results, a dominant contribution of electrostatic components to the binding energy and a pronounced effect of the N138A, and especially R131A mutation on the electrostatic energy, were also revealed through MD simulations.

Similar ionicity-dependent effects on binding kinetics have been shown for other interactions in the complement system, such as the binding of components C2 and C4b (Laich and Sim 2001) or the recognition of C3d by complement receptor 2 (CR2) (Sarrias et al. 2001). In the latter case, mutation studies (Clemenza and Isenman 2000; Hannan et al. 2005), as well as computational (Morikis and Lambris 2004) and structural analyses (Nagar et al. 1998; Szakonyi et al. 2001; Gilbert et al. 2005), all confirmed the large involvement of electrostatic contributions, although with some discrepancies on the exact localization of the interaction site. Another impres-

sive example of electrostatic interactions between microbial evasion proteins and their target in the complement systems has been reported for the viral inhibitors VCP (vaccinia virus complement control protein) and SPICE (smallpox inhibitor of complement enzymes), where differences in the electrostatic potential between these highly similar proteins seem to be responsible for a 1000-fold difference in their inhibitory functions (Sfyrera et al. 2005). These examples further undermine the importance of electrostatic attraction and ion pair networks for the function and attenuation of the complement system.

Detailed computational analysis of pairwise interactions not only reiterated the importance of Arg-131 and Asn-138, but also allowed us to identify potential contributions of other residues for the interaction between Efb-C and C3d. The majority of these residues were found to form H-bonds and salt bridges, which presumably contribute to the stability of the complex. However, some of the identified interaction pairs are predominantly hydrophobic or involve the backbones of hydrophobic residues. In many cases, these interactions involve residues that at first glance did not appear to be essential for either formation or maintenance of the Efb-C/C3d

complex. Thus, in conjunction with our previous mass spectrometry-based experiments that identified binding areas outside the visible range of the cocrystal structure (Chen et al. 2008), the approaches and results presented here constitute a valuable extension in our understanding of the Efb-C/C3d interface. In addition to facilitating a systematic mutagenesis of these residues, this work also highlights the highly cooperative framework that drives specific protein–protein interactions.

The multifaceted and highly efficient actions of the human complement system are maintained by a host of carefully timed and regulated enzymatic cleavages and protein–protein interactions (Ricklin and Lambris 2007b). But despite large efforts by academic and pharmaceutical groups, targeted inhibition of these proteases has not led to successful clinical therapeutics. As a consequence, recent progress in the field has focused mainly on the disruption of protein–protein interactions, with the successful marketing of a complement-specific antibody in 2007 (Ricklin and Lambris 2007a). Though biopharmaceuticals (e.g., monoclonal antibodies and soluble proteins) will continue to provide a majority of protein–protein interaction inhibitors, recent reports have also suggested that peptides and small molecules may well be capable of modulating large interaction interfaces when binding to so-called hot spots (Wells and McClendon 2007). To design smaller and less immunogenic peptides that mimic the function of naturally occurring inhibitory proteins such as Efb-C, a detailed knowledge of the residues found at such hot spots in terms of their physical–chemical contributions to these interactions is essential. Though the work presented here will certainly guide optimization of Efb-C-based complement inhibitors, it also demonstrates more generally that employment of a multidisciplinary approach in interface analysis and inhibitor design can provide valuable information complementary to more traditional structural and combinatorial-based efforts.

Materials and Methods

Preparation of recombinant proteins

A recombinant form of human complement fragment C3d was expressed and purified according to a previously described adaptation of the original procedure of Nagar et al. (Nagar et al. 1998; Hammel et al. 2007b). Plasmids encoding site-directed alanine mutations of Efb-C residues Arg-131 (R131A) or Asn-138 (N138A) were prepared using a two-step megaprimer method as previously described (Hammel et al. 2007b). All forms of Efb-C used during these studies were expressed and purified in a manner identical to that used in preparation of wild-type Efb-C (Hammel et al. 2007b). Prior to further analysis, the structural integrity of all mutant proteins was assessed by circular dichroism spectropolarimetry.

Crystallization, X-ray diffraction analysis, structure solution, and refinement

Crystallization of C3d-bound complexes for both the R131A and N138A mutants of Efb-C was performed identically to that for wild-type Efb-C (Hammel et al. 2007b). Briefly, protein complexes were reconstituted by incubating 1:2 molar ratios of purified C3d with the respective Efb-C mutant for 10 min at room temperature. Following removal of residual Efb-C by gel filtration chromatography, the isolated complexes were dialyzed against double-deionized water and concentrated to 3.8 mg/mL and 5.1 mg/mL total protein for the R131A and N138A complexes, respectively. Cube-shaped crystals were obtained within 3–5 d at room temperature by vapor diffusion of hanging drops that consisted of 1 μ L protein solution and 1 μ L 60% tacsimate, pH 7.0, and that were equilibrated over a well solution of 60% tacsimate, pH 7.0.

Following harvest, crystals were soaked briefly in a solution of 100% tacsimate, pH 7.0, and flash frozen in liquid nitrogen. All X-ray diffraction analyses of frozen crystal samples were performed at SER-CAT beamline 22-ID at the Advanced Photon Source of Argonne National Laboratory. Cell content analyses in the tetragonal space group $P4_1$ were consistent with two unique complexes in the asymmetric unit of each cocrystal. As a result, both structures were solved by molecular replacement (MOLREP) using a search model comprised of both complete Efb-C/C3d complexes present in the refined asymmetric unit of the wild-type structure (PDB accession code 2GOX) (Collaborative Computational Project Number 4 1994). Refinement was conducted in a stepwise fashion using the rigid-body, conjugate gradient minimization and individual B-factor protocols of CNS, followed by a final round of solvent addition using the same software suite (Brunger et al. 1998). Complete details regarding areas of weak/missing density and corresponding residues that could not be modeled can be found in the respective PDB (Bernstein et al. 1977) files. The refined coordinates and structure factors for each complex have been deposited in the PDB under accession codes 3D5R (N138A/C3d) and 3D5S (R131A/C3d).

Coordinate superpositions of the refined wild-type and mutant Efb-C/C3d complexes were prepared using the Local/Global Alignment method and default parameters (<http://as2ts.llnl.gov/>) (Zemla 2003). Following this, figures of superimposed complexes were generated in PyMOL (DeLano Scientific).

Isothermal titration calorimetry experiments

Thermodynamic characterization of the interaction between C3d and the various Efb-C proteins was performed at 25°C in 20 mM Tris pH 8.0, 200 mM NaCl using a VP-ITC calorimeter (MicroCal LLC). Multiple injections of 5 μ L Efb-C samples (150 μ M) were performed into C3d in the sample cell (12 μ M) at 240-sec intervals. Buffer titration baseline values were subtracted from the resulting thermogram and binding enthalpy (ΔH), and affinity (K_d) values were extracted by fitting the data to a single set of sites in Origin (OriginLab). Entropy ($-T\Delta S$) and Gibbs free energy (ΔG) values were calculated using the following set of relationships:

$$\Delta G = \Delta H - T\Delta S = RT \ln K_D.$$

Surface plasmon resonance experiments

All SPR experiments were performed on a Biacore 2000 instrument (Biacore Inc.) at 25°C using research-grade carboxymethyl

dextran sensor chips (CM5). Wild-type and mutant Efb-C proteins were immobilized at equal surface density (215–240 RU) on separate flow cells of the sensor chip by standard amine coupling using activation and deactivation contact times of 5 min each. An activated and deactivated flow cell has been used as a reference surface for subtracting bulk solvent signals. C3d (22–0.27 nM) was twofold serially diluted in running buffer (10 mM sodium phosphate, 150 mM sodium chloride, 0.005% Tween-20, pH 7.4) and samples were injected for 5 min at a flow rate of 20 μ L/min. Analyte dissociation was observed for 5 min before the surface was regenerated with two consecutive injections of 0.1% SDS and reconstituted for 10 min in running buffer before the next injection. Data processing was performed using Scrubber (BioLogic Software Pty Ltd.). Baselines and injection start points were adjusted, and the signals were double referenced by subtracting an ensemble of buffer blank injections. Kinetic rate constants (k_{on} , k_{off}) were determined by globally fitting the binding curves to a Langmuir 1:1 binding model and used for the calculation of the dissociation constant ($K_d = k_{\text{off}}/k_{\text{on}}$). The values in Table 2 represent the average of three independent data sets.

For electrostatic titration experiments, the C3d injection series described above were repeated in running buffers of increasing sodium chloride concentration (10 mM sodium phosphate pH 7.4 with 75, 150, 300, and 600 mM NaCl, respectively). The pH of all running buffers was carefully adjusted after addition of NaCl. Semiquantitative analysis of the association and dissociation phases was performed by overlaying the processed binding signals at 22 nM C3d for all ionic strengths.

Molecular dynamics setup

The wild-type structure was taken from the PDB (accession code 2GOX). The N138A and R131A mutant complexes were taken from the crystallographic data (see above). Missing side chains from the PDB files, as well as hydrogen atoms, have been added using AMBER 9 leap utility (Pearlman et al. 1995; Case et al. 2006). The simulations were conducted using the AMBER ff03 force field (Duan et al. 2003). The molecules were represented at the fully atomic level. Implicit solvent was used via the General Born solvation method, as implemented by Hawkins et al. (1995, 1996) and Tsui and Case (2000). Minimization was done for 5000 steps, the first 2500 steps using the steepest descent method (Arfken 1985) and the last 2500 using conjugate gradients (Hestenes and Stiefel 1952; Fletcher and Reeves 1964). Minimization was followed by 20 psec of gradual heating to 300 K and equilibration. The MD simulations were performed for 20 nsec at a constant temperature of 300 K. The SHAKE algorithm, as implemented by Miyamoto and Kollman (1992) was used to restrain the length of bonds involving hydrogen. This allowed an integration time step of 2 fsec.

The trajectory analysis was performed by the ptraj tool, which is a part of the AMBER package. The plots were generated using MatLab and the figures were generated using VMD (Humphrey et al. 1996). The sequence alignment was done by the Clustalx package (Thompson et al. 1997).

Free energy of binding

The free energy of the complex was estimated using the mm-pbsa/gbsa approach (Kollman et al. 2000) implemented as a part of the AMBER package.

The average complex binding energy is obtained by the following formula:

$$\Delta G_{\text{binding}} = G_{\text{total,complex}} - G_{\text{total,C3D}} - G_{\text{total,Efb-C}}$$

where

$$G_{\text{total}} = \Delta E_{\text{MM,gas}} + \Delta \Delta G_{\text{solv}} - T\Delta S$$

where $\Delta E_{\text{MM,gas}}$ is the gas phase molecular mechanics energy, $\Delta \Delta G_{\text{solv}}$ is the change in the free energy upon solvation, and $T\Delta S$ is the contribution of the entropic effect to the free energy. In this study, the entropy was not calculated due to exceedingly high computational demands.

The solvation free energy (ΔG_{solv}) is the sum of two terms, the electrostatic contribution and the nonpolar contribution:

$$\Delta G_{\text{solv}} = \Delta G_{\text{el}} + \Delta G_{\text{np}}$$

The electrostatic contribution to the solvation energy was estimated using the General Born method (Still et al. 1990; Srinivasan et al. 1999). The nonpolar solvation term (ΔG_{np}) was calculated from the solvent-accessible surface area (SASA), which is estimated using the LPCO method (Weiser et al. 1999). γ was set to 0.0072 kcal/(mol \cdot \AA^2) and $\beta = 0$ kcal/mol in the following equation:

$$\Delta G_{\text{np}} = \gamma * \text{SASA} + \beta$$

In the mm-pbsa/gbsa approach, the average free energy is calculated on an ensemble of uncorrelated snapshots extracted from the equilibrated simulation. In this study, a snapshot was taken every 10 psec for the molecular mechanics and solvation components. The first 2 nsec of simulation were not considered for free energy calculation, to make sure the system had equilibrated. This resulted in 1800 samples.

Binding free energy calculations were done using the single protein-ligand trajectory approximation. This means that the C3d and Efb-C molecules were not simulated separately, but rather the snapshot structures for the energy calculations of the C3d-Efb-C complex and separated C3d and Efb-C were taken from the MD trajectory of the Efb-C/C3d complex. This protocol has been used extensively to estimate the binding of protein-protein, as well as protein-DNA or protein-RNA complexes, as demonstrated, for example, by Laitinen et al. (2004), Onufriev et al. (2004), and Trieb et al. (2004). We used the default dielectric constants of $\epsilon = 1$ for the solute and $\epsilon = 80$ for the solvent in the electrostatic solvation free energy (ΔG_{GB}) calculations. A probe radius of 1.4 \AA was used to determine the molecular surface area.

Electrostatic potential surface

The electrostatic potential surface was evaluated using the adaptive Poisson-Boltzmann solver (APBS) software (Holst and Saied 1993, 1995; Baker et al. 2001). This software calculates the potential surface by providing a numerical solution to the Poisson-Boltzmann equation using a grid-based approach.

Acknowledgments

We thank Zhongmin Jin for expert technical assistance during diffraction data collection. Use of the Advanced Photon Source was supported by the U.S. Department of Energy, Office of Science, Office of Basic Energy Sciences, under Contract No. W-31-109-Eng-38. Data were collected at Southeast Regional Collaborative Access Team (SER-CAT) 22-ID beamline at the Advanced Photon Source, Argonne National Laboratory. A list of supporting member institutions may be found at www.ser-cat.org/members.html.

This work has been supported by the National Institutes of Health (Grant No. GM078988, AI071028, and P01AI68730), the National Science Foundation (Grant No. 0523908), and the Sloan Foundation. Computational experiments were conducted on the Rice Computational Research Cluster funded by the National Science Foundation under Grant No. CNS-0421109 and Grant No. CNS-0454333, and a partnership between Rice University, AMD, and Cray.

References

- Arfken, G. 1985. The method of steepest descents. In *Mathematical methods for physicists*, 3rd ed., pp. 428–436. Academic Press, Orlando, FL.
- Baker, N.A., Sept, D., Joseph, S., Holst, M.J., and McCammon, J.A. 2001. Electrostatics of nanosystems: Application to microtubules and the ribosome. *Proc. Natl. Acad. Sci.* **98**: 10037–10041.
- Bernstein, F.C., Koetzle, T.F., Williams, G.J., Meyer Jr., E.F., Brice, M.D., Rodgers, J.R., Kennard, O., Shimanouchi, T., and Tasumi, M. 1977. The Protein Data Bank: A computer-based archival file for macromolecular structures. *J. Mol. Biol.* **112**: 535–542.
- Bonnet, P. and Bryce, R.A. 2005. Scoring binding affinity of multiple ligands using implicit solvent and a single molecular dynamics trajectory: Application to influenza neuraminidase. *J. Mol. Graph. Model.* **24**: 147–156.
- Brunger, A.T., Adams, P.D., Clore, G.M., DeLano, W.L., Gros, P., Grosse-Kunstleve, R.W., Jiang, J.S., Kuszewski, J., Nilges, M., Pannu, N.S., et al. 1998. Crystallography & NMR system: A new software suite for macromolecular structure determination. *Acta Crystallogr. D Biol. Crystallogr.* **54**: 905–921.
- Carroll, M.C. 2000. The role of complement in B cell activation and tolerance. *Adv. Immunol.* **74**: 61–88.
- Case, D.A., Darden, T.A., Cheatham III, T.E., Simmerling, C.L., Wang, J., Duke, R.E., Luo, R., Merz, K.M., Pearlman, D.A., and Crowley, M., et al. 2006. AMBER 9. University of California, San Francisco.
- Chavakis, T., Preissner, K.T., and Herrmann, M. 2007. The anti-inflammatory activities of *Staphylococcus aureus*. *Trends Immunol.* **28**: 408–418.
- Chen, H., Schuster, M.C., Sfyroera, G., Geisbrecht, B.V., and Lambris, J.D. 2008. Solution insights into the structure of the Efb/C3 complement inhibitory complex as revealed by lysine acetylation and mass spectrometry. *J. Am. Soc. Mass Spectrom.* **19**: 55–65.
- Clemenza, L. and Isenman, D.E. 2000. Structure-guided identification of C3d residues essential for its binding to complement receptor 2 (CD21). *J. Immunol.* **165**: 3839–3848.
- Collaborative Computational Project Number 4. 1994. The CCP4 suite: Programs for protein crystallography. *Acta Crystallogr. D Biol. Crystallogr.* **50**: 760–763.
- Duan, Y., Wu, C., Chowdhury, S., Lee, M.C., Xiong, G., Zhang, W., Yang, R., Cieplak, P., Luo, R., Lee, T., et al. 2003. A point-charge force field for molecular mechanics simulations of proteins based on condensed-phase quantum mechanical calculations. *J. Comput. Chem.* **24**: 1999–2012.
- Edinger, S.R., Cortis, C., Shenkin, P.S., and Friesner, R.A. 1997. Solvation free energies of peptides: Comparison of approximate continuum solvation models with accurate solution of the Poisson-Boltzmann equation. *J. Phys. Chem. B* **101**: 1190–1197.
- Fletcher, R. and Reeves, C.M. 1964. Function minimization by conjugate gradients. *Comput. J.* **7**: 149. doi: 10.1093/comjnl/7.2.149.
- Foster, T.J. 2005. Immune evasion by staphylococci. *Nat. Rev. Microbiol.* **3**: 948–958.
- Gilbert, H.E., Eaton, J.T., Hannan, J.P., Holers, V.M., and Perkins, S.J. 2005. Solution structure of the complex between CR2 SCR 1-2 and C3d of human complement: An X-ray scattering and sedimentation modelling study. *J. Mol. Biol.* **346**: 859–873.
- Hammel, M., Sfyroera, G., Pyrpasopoulos, S., Ricklin, D., Ramyar, K.X., Pop, M., Jin, Z., Lambris, J.D., and Geisbrecht, B.V. 2007a. Characterization of Ehp, a secreted complement inhibitory protein from *Staphylococcus aureus*. *J. Biol. Chem.* **282**: 30051–30061.
- Hammel, M., Sfyroera, G., Ricklin, D., Magotti, P., Lambris, J.D., and Geisbrecht, B.V. 2007b. A structural basis for complement inhibition by *Staphylococcus aureus*. *Nat. Immunol.* **8**: 430–437.
- Hannan, J.P., Young, K.A., Guthridge, J.M., Asokan, R., Szakonyi, G., Chen, X.S., and Holers, V.M. 2005. Mutational analysis of the complement receptor type 2 (CR2/CD21)-C3d interaction reveals a putative charged SCR1 binding site for C3d. *J. Mol. Biol.* **346**: 845–858.
- Hawkins, G.D., Cramer, C.J., and Truhlar, D.G. 1995. Pairwise solute descreening of solute charges from a dielectric medium. *Chem. Phys. Lett.* **246**: 122–129.
- Hawkins, G.D., Cramer, C.J., and Truhlar, D.G. 1996. Parametrized models of aqueous free energies of solvation based on pairwise descreening of solute atomic charges from a dielectric medium. *J. Phys. Chem.* **100**: 19824–19839.
- Hestenes, M.R. and Stiefel, E. 1952. Methods of conjugate gradients for solving linear systems. *J. Res. Natl. Bur. Stand.* **49**: 409–436.
- Holst, M. and Saied, F. 1993. Multigrid solution of the Poisson-Boltzmann equation. *J. Comput. Chem.* **14**: 105–113.
- Holst, M.J. and Saied, F. 1995. Numerical-solution of the nonlinear Poisson-Boltzmann equation—developing more robust and efficient methods. *J. Comput. Chem.* **16**: 337–364.
- Humphrey, W., Dalke, A., and Schulten, K. 1996. VMD: Visual molecular dynamics. *J. Mol. Graph.* **14**: 33.
- Janssen, B.J., Christodoulidou, A., McCarthy, A., Lambris, J.D., and Gros, P. 2006. Structure of C3b reveals conformational changes that underlie complement activity. *Nature* **444**: 213–216.
- Jongierius, I., Kohl, J., Pandey, M.K., Ruyken, M., van Kessel, K.P., van Strijp, J.A., and Rooijackers, S.H. 2007. Staphylococcal complement evasion by various convertase-blocking molecules. *J. Exp. Med.* **204**: 2461–2471.
- Kollman, P.A., Massova, I., Reyes, C., Kuhn, B., Huo, S., Chong, L., Lee, M., Lee, T., Duan, Y., Wang, W., et al. 2000. Calculating structures and free energies of complex molecules: Combining molecular mechanics and continuum models. *Acc. Chem. Res.* **33**: 889–897.
- Laich, A. and Sim, R.B. 2001. Complement C4bC2 complex formation: An investigation by surface plasmon resonance. *Biochim. Biophys. Acta* **1544**: 96–112.
- Laitinen, T., Kankare, J.A., and Perakyla, M. 2004. Free energy simulations and MM-PBSA analyses on the affinity and specificity of steroid binding to antiestradiol antibody. *Proteins* **55**: 34–43.
- Lambris, J.D., Ricklin, D., and Geisbrecht, B.V. 2008. Complement evasion by human pathogens. *Nat. Rev. Microbiol.* **6**: 132–142.
- Lee, L.Y., Hook, M., Haviland, D., Wetsel, R.A., Yonter, E.O., Srybelys, P., Vernachio, J., and Brown, E.L. 2004a. Inhibition of complement activation by a secreted *Staphylococcus aureus* protein. *J. Infect. Dis.* **190**: 571–579.
- Lee, L.Y., Liang, X., Hook, M., and Brown, E.L. 2004b. Identification and characterization of the C3 binding domain of the *Staphylococcus aureus* extracellular fibrinogen-binding protein (Efb). *J. Biol. Chem.* **279**: 50710–50716.
- Miyamoto, S. and Kollman, P.A. 1992. Settle: An analytical version of the SHAKE and RATTLE algorithm for rigid water models. *J. Comput. Chem.* **13**: 952–962.
- Morikis, D. and Lambris, J.D. 2004. The electrostatic nature of C3d-complement receptor 2 association. *J. Immunol.* **172**: 7537–7547.
- Nagar, B., Jones, R.G., Diefenbach, R.J., Isenman, D.E., and Rini, J.M. 1998. X-ray crystal structure of C3d: A C3 fragment and ligand for complement receptor 2. *Science* **280**: 1277–1281.
- Nordahl, E.A., Rydengard, V., Nyberg, P., Nitsche, D.P., Morgelin, M., Malmsten, M., Bjorck, L., and Schmidtchen, A. 2004. Activation of the complement system generates antibacterial peptides. *Proc. Natl. Acad. Sci.* **101**: 16879–16884.
- Onufriev, A., Bashford, D., and Case, D.A. 2004. Exploring protein native states and large-scale conformational changes with a modified generalized born model. *Proteins* **55**: 383–394.
- Pearlman, D.A., Case, D.A., Caldwell, J.W., Ross, W.S., Cheatham, T.E., Debolt, S., Ferguson, D., Seibel, G., and Kollman, P. 1995. AMBER, a package of computer-programs for applying molecular mechanics, normal-mode analysis, molecular-dynamics and free-energy calculations to simulate the structural and energetic properties of molecules. *Comput. Phys. Commun.* **91**: 1–41.
- Ricklin, D. and Lambris, J.D. 2007a. Complement-targeted therapeutics. *Nat. Biotechnol.* **25**: 1265–1275.

- Ricklin, D. and Lambris, J.D. 2007b. Exploring the complement interaction network using surface plasmon resonance. *Adv. Exp. Med. Biol.* **598**: 260–278.
- Sahu, A. and Lambris, J.D. 2001. Structure and biology of complement protein C3, a connecting link between innate and acquired immunity. *Immunol. Rev.* **180**: 35–48.
- Sarrias, M.R., Franchini, S., Canziani, G., Argyropoulos, E., Moore, W.T., Sahu, A., and Lambris, J.D. 2001. Kinetic analysis of the interactions of complement receptor 2 (CR2, CD21) with its ligands C3d, iC3b, and the EBV glycoprotein gp350/220. *J. Immunol.* **167**: 1490–1499.
- Sfyroera, G., Katragadda, M., Morikis, D., Isaacs, S.N., and Lambris, J.D. 2005. Electrostatic modeling predicts the activities of orthopoxvirus complement control proteins. *J. Immunol.* **174**: 2143–2151.
- Sinha, N. and Smith-Gill, S.J. 2002. Electrostatics in protein binding and function. *Curr. Protein Pept. Sci.* **3**: 601–614.
- Srinivasan, J., Trevathan, M.W., Beroza, P., and Case, D.A. 1999. Application of a pairwise Generalized Born model to proteins and nucleic acids: Inclusion of salt effects. *Theor. Chem. Accts.* **101**: 426–434.
- Still, W.C., Tempczyk, A., Hawley, R.C., and Hendrickson, T. 1990. Semi-analytical treatment of solvation for molecular mechanics and dynamics. *J. Am. Chem. Soc.* **112**: 6127–6129.
- Szakonyi, G., Guthridge, J.M., Li, D., Young, K., Holers, V.M., and Chen, X.S. 2001. Structure of complement receptor 2 in complex with its C3d ligand. *Science* **292**: 1725–1728.
- Thompson, J.D., Gibson, T.J., Plewniak, F., Jeanmougin, F., and Higgins, D.G. 1997. The CLUSTAL_X windows interface: Flexible strategies for multiple sequence alignment aided by quality analysis tools. *Nucleic Acids Res.* **25**: 4876–4882.
- Trieb, M., Rauch, C., Wibowo, F.R., Wellenzohn, B., and Liedl, K.R. 2004. Cooperative effects on the formation of intercalation sites. *Nucleic Acids Res.* **32**: 4696–4703.
- Tsui, V. and Case, D.A. 2000. Theory and applications of the Generalized Born solvation model in macromolecular simulations. *Biopolymers* **56**: 275–291.
- Weiser, J., Shenkin, P.S., and Still, W.C. 1999. Approximate atomic surfaces from linear combinations of pairwise overlaps (LCPO). *J. Comput. Chem.* **20**: 217–230.
- Wells, J.A. and McClendon, C.L. 2007. Reaching for high-hanging fruit in drug discovery at protein–protein interfaces. *Nature* **450**: 1001–1009.
- Zemla, A. 2003. LGA: A method for finding 3D similarities in protein structures. *Nucleic Acids Res.* **31**: 3370–3374.